

引用格式: LI Yi-Hsun, KUO Chun-Yi, HUANG Sheng-Lung. Transition-metal-ion Doped Tunable Crystalline Fiber Lasers (Invited)[J]. *Acta Photonica Sinica*, 2020, 49(11):1149010

李奕勋,郭俊毅,黄升龙. 过渡金属离子掺杂的可调频晶体光纤激光器(特邀)[J]. 光子学报, 2020, 49(11):1149010

## 过渡金属离子掺杂的可调频晶体光纤 激光器(特邀)

李奕勋, 郭俊毅, 黄升龙

(台湾大学 电机系暨光电所, 台北 10617)

**摘 要:** 宽带可调频激光器除了可用于基础的光谱学研究外, 也可应用于各式光通信乃至生物医学成像. 过渡金属离子掺杂的固体激光器特别适用于宽频光源的产生, 掺钛蓝宝石及掺铬石榴石晶体是目前广为应用的两个例子, 将其生长成晶体光纤并以玻璃包覆的激光器在红外光波段展现了优异的特性. 掺钛蓝宝石晶体光纤激光器具有高光转换效率、低阈值且调频范围可达 180 nm; 掺铬石榴石晶体光纤激光器的可调频范围亦达到了 170 nm, 被激发态吸收所限制. 为了纪念激光器发明 60 周年, 本文简要回顾了过渡金属离子掺杂的固体激光器的发展, 并介绍了晶体光纤激光器最新的成果. 分析了掺钛蓝宝石晶体光纤激光器的调频速率, 并与掺铬石榴石晶体光纤的光学特性做了实验与数值模拟的比较. 目前逐渐成熟的玻璃包覆晶体光纤激光器, 预期在超宽频光通信及细胞级分辨率的光学相干断层扫描术方面有很大的应用潜力.

**关键词:** 晶体光纤; 激光器; 掺钛蓝宝石; 掺铬石榴石; 宽带光通信; 生医影像

中图分类号: TN248.1; TN253

文献标识码: A

doi:10.3788/gzxb20204911.1149010

### Transition-metal-ion Doped Tunable Crystalline Fiber Lasers (Invited)

LI Yi-Hsun, KUO Chun-Yi, HUANG Sheng-Lung

(Graduate Institute of Photonics and Optoelectronics, Taiwan University, Taipei 10617, China)

**Abstract:** Broadly tunable lasers are useful for basic spectroscopy studies, as well as a wide range of applications from optical communications to biomedical imaging. Transition-metal-ions doped solid-state gain media are eminently suitable for generating broadband emissions.  $Ti^{3+}$ : sapphire and  $Cr^{4+}$ : YAG crystals are 2 successful examples that are now widely used. Glass-clad  $Ti^{3+}$ : sapphire and  $Cr^{4+}$ : YAG crystal fibers have shown superior performance for broadly tunable lasers in the near infrared wavelength ranges. The tunable  $Ti^{3+}$ : sapphire crystal fiber lasers are efficient, and have demonstrated the lowest threshold over a 180 nm tuning range. The  $Cr^{4+}$ : YAG crystal fiber laser shows a tuning range of 170 nm, limited by the excited state absorption. To celebrate the 60<sup>th</sup> anniversary since laser invention, a brief historical review and the latest developments of the  $Ti^{3+}$ : sapphire and  $Cr^{4+}$ : YAG crystal fiber lasers are discussed in the manuscript. The tunable  $Ti^{3+}$ : sapphire crystal fiber laser's wavelength sweeping speed is envisioned, and the optical properties are compared with that of the  $Cr^{4+}$ : YAG crystal fiber. With well-developed crystalline cores and clads for broadly tunable lasers, it is expected that novel applications, such as ultra-broadband optical fiber communications and cellular-resolution optical coherence tomography,

**First author:** LI Yi-Hsun (1994-), male, engineer, M.S. degree, mainly focuses on crystal fiber lasers. Email: lo5yb72e@gmail.com

**Supervisor (Contact author):** HUANG Sheng-Lung (1964-), male, professor, Ph.D. degree, mainly focuses on crystal fiber based lasers and biomedical imaging. Email: shuang@ntu.edu.tw

**Received:** Aug.31, 2020; **Accepted:** Sep.19, 2020

<http://www.photon.ac.cn>

could be evolved to meet the high data rate and high image resolution needs in future.

**Key words:** Crystal fiber; Laser;  $\text{Ti}^{3+}$  : sapphire;  $\text{Cr}^{4+}$  : YAG; Broadband optical communication; Biomedical imaging

**OCIS Codes:** 160.2290; 140.3580; 140.5680; 060.2330; 170.4500

## 0 Introduction

Since the invention of laser by MAIMAN T in 1960, laser technology advancement and application development have moving forward at a very fast pace over the past 60 years. In addition to the applications benefitted by laser's high monochromaticity, broadband laser sources have also made significant progresses ranging from optical communications<sup>[1-2]</sup> to biomedical imaging applications<sup>[3-4]</sup>. It is well known that transition-metal-ions doped solid-state lasers exhibit broadband emissions due to the strong interaction of the electronic states with lattice phonons<sup>[5-6]</sup>. The interaction leads to a strong homogeneous broadening of the transition and thus results in a broad gain bandwidth. The broad gain bandwidth, however, inherently exhibits small product of emission cross section and fluorescent lifetime<sup>[7]</sup>. As a result, one major limitation for transition metal ions doped lasers has been the high pump-power density required for efficient lasing<sup>[8]</sup>. Efforts have, therefore, been directed toward waveguide fabrication in transition-metal-ion doped crystals, since the simultaneous pump- and signal-beam confinement leads to average spot sizes that are not obtainable in bulk, with an associated reduction in lasing threshold. The requirement is to fabricate waveguide layers of high crystal quality and low scattering loss, which would allow the use of laser diode pump sources. The development of the optical waveguiding in the 1970s activated the further growth of single Crystalline Fiber (CF) for diversified applications. It has been over 40 years since CF was first used as the laser gain media<sup>[9-10]</sup>. Through the advancement of the growth techniques on the crystalline core<sup>[11-12]</sup>, high quality CFs enable its gradual penetration into various dopants, hosts, and applications. In terms of geometric shape, it is well known that fiber structure has the largest surface to volume ratio, which is advantageous for light source to dissipate heat from quantum defect and other non-radiative losses. The CF could make possible optical devices that cannot be realized in glass fibers or bulk crystalline media. Linear polarized fiber laser was demonstrated using birefringent crystal fiber as the gain medium<sup>[13-14]</sup>. The broad transmission window and high melting point of many crystalline materials make them attractive for tunable lasers as well as high brightness low-coherent light sources. The Laser-Heated Pedestal Growth (LHPG) method is now a well-established technique for the growth of single-crystal fibers<sup>[15]</sup>. It is crucible free and can, therefore, produce high-purity, low-defect density single crystals with small diameter and long length. Cladding the CF reduces both scattering loss and the number of propagating modes. Various cladding techniques have been developed over the past 20 years<sup>[16-18]</sup>. Following the historical path of silica fibers, few mode, single mode, as well as double-clad CFs are advancing rapidly in recent years using the co-drawing LHPG method<sup>[19]</sup>. By far, the lowest propagation loss of crystalline waveguide was achieved by the Glass-Clad CFs (GCCFs) prepared by the LHPG method<sup>[20]</sup>. Among the broadly tunable laser gain media,  $\text{Ti}^{3+}$  : sapphire and  $\text{Cr}^{4+}$  : YAG are the very few that were draw into GCCFs to improve the laser characteristics in terms of heat dissipation, pump/signal mode matching, interaction length, and cost reduction.

$\text{Ti}^{3+}$  : sapphire crystal was first demonstrated as a widely tunable laser gain medium at the Lincoln Laboratory<sup>[21]</sup>. The  $\text{Ti}^{3+}$  : sapphire crystals used in the initial experiments exhibited significant scattering and an unidentified absorption at the laser wavelength. These losses affected the efficiency of the laser, and only pulsed operation was possible. As high-quality crystals became available, a series of tunable lasers based upon  $\text{Ti}^{3+}$  : sapphire appeared, and a 235 nm tuning bandwidth was demonstrated with one mirror set<sup>[22]</sup>. For waveguide  $\text{Ti}^{3+}$  : sapphire lasers, continuous-wave channel waveguide lasers were demonstrated and the emission wavelength was tuned over a 170 nm range by using a birefringent filter in an external cavity<sup>[23]</sup>.

Among all the  $\text{Cr}^{4+}$  doped gain media,  $\text{Cr}^{4+}$  : YAG has been shown high concentration of tetrahedrally coordinated  $\text{Cr}^{4+}$  ions and high emission cross section in fiber communication bands.  $\text{Cr}^{4+}$  : YAG tunable laser has been developed for thirty years, and the first demonstrated was operated in gain-switched mode with a tuning range from 1.35 to 1.45  $\mu\text{m}$ <sup>[24]</sup>. Then, there were tunable lasers been demonstrated in continuous-wave mode<sup>[25]</sup>. These systems used high power solid-state laser as pumping source, which was massive and high cost. Although laser diode could reduce the cost and volume, the threshold was still in the Watt level<sup>[26]</sup>. Another

issue was the thermal loading in crystal with bulk structure. The lifetime would suffer from the thermal loading and the thermal lensing effect in the crystal<sup>[27]</sup>. To overcome the thermal problem and poor pump/signal beam overlapping in bulk crystal, a 120  $\mu\text{m}$ -diameter  $\text{Cr}^{4+}$ :YAG crystal fiber was developed with a tuning range of 180 nm at a threshold pump power above 2 W<sup>[28]</sup>.

By far, active glass-clad crystal fibers have shown the state-of-the-art performance among transition-metal-ions doped solid-state waveguide lasers<sup>[29-31]</sup>. In this paper, the latest development of glass-clad  $\text{Ti}^{3+}$ :sapphire and  $\text{Cr}^{4+}$ :YAG crystalline fibers based tunable lasers are presented with a focus on the tuning range and wavelength sweeping capabilities.

## 1 Crystal fiber growth and cladding

Various oxide crystals have been drawn into the fiber forms. For Ti:sapphire and Cr:YAG crystals, the melting points are 2 050 °C and 1 970 °C, respectively. The high melting points make LHPG advantageous to avoid crucible contamination. As shown in Fig. 1(a), an expanded  $\text{CO}_2$  laser beam entered the growth chamber and was converted into a donut shape by the reflexicon. It was then focused by the paraboloidal mirror onto the CF. The inner cone was supported by a ZnSe plate, which is transparent to  $\text{CO}_2$  laser beam. The 360° axial symmetry prevented cold spots in the growth molten zone. The source and the seed crystal rods were fixed on the lower and upper motorized stages. During stable growth, the dependence of the molten-zone length and shape on the heating  $\text{CO}_2$  laser were analyzed under both the maximum and the minimum allowed powers<sup>[32]</sup>. To avoid the high convection rate inside the floating molten zone due to mass-transfer and thermocapillary convections, the  $\text{CO}_2$  laser stability and the mechanical resonant of the motorized stage should be well controlled to produce high quality grown fibers. Due to the long  $\text{CO}_2$  laser wavelength, it is difficult to reduce the fiber diameter down to 10  $\mu\text{m}$  by direct focused heating. The co-drawing approach has shown core diameter in the order of 10  $\mu\text{m}$ . In the co-drawing method, the crystalline core was prepared by the LHPG technique, while the claddings were made from various glass capillaries, such as borosilicate, aluminosilicate, flint glass, or even high temperature fused silica. Using YAG Double-Clad Crystal Fiber (DCCF) growth as an example, a schematic of the co-drawing LHPG technique is depicted as shown in Fig.1(b). With two diameter reduction steps by the LHPG technique, 68  $\mu\text{m}$ -diameter YAG single CFs were initially prepared from a 0.5 mol.% doped Cr:YAG source rod in  $\langle 111 \rangle$  crystal orientation with a cross section of 500  $\mu\text{m} \times 500 \mu\text{m}$ . When the

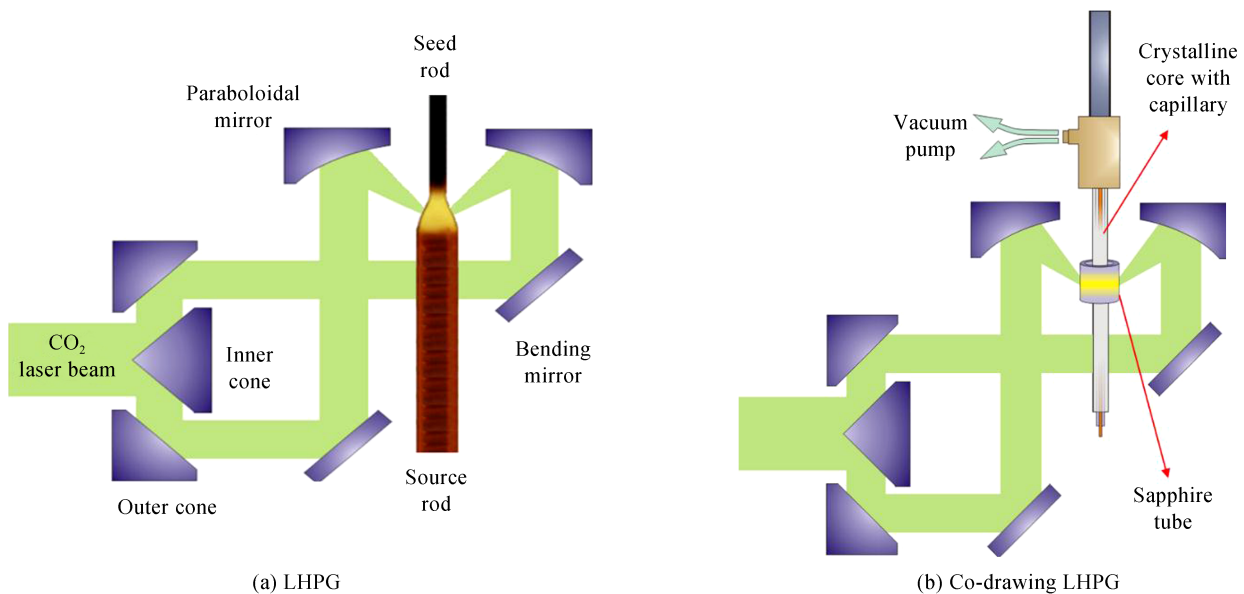


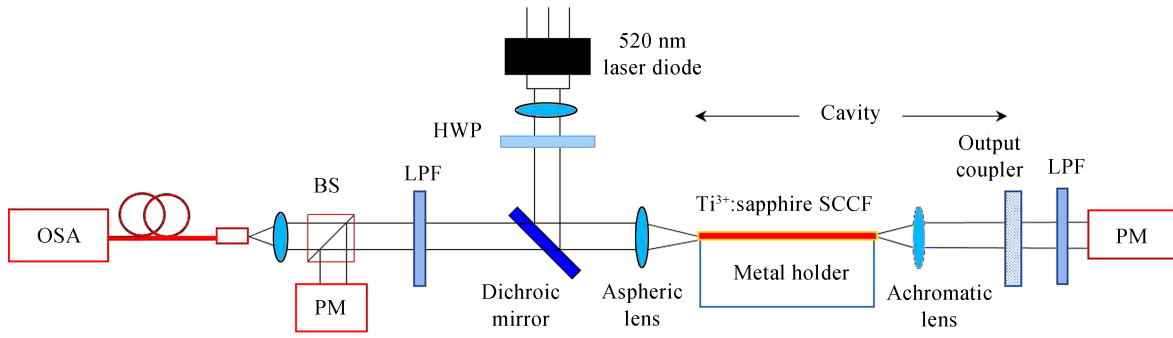
Fig. 1 The LHPG and co-drawing LHPG schemes

Cr:YAG CFs were grown at a lower speed, nonepitaxial  $\text{Cr}_{3-\delta}\text{O}_4$  crystallites with spinel-type structure were formed on the  $\{112\}$  side surfaces. The deposition of  $\text{Cr}_{3-\delta}\text{O}_4$ , rather than segregation of Cr and Ca codopants, can be rationalized by a high crystal field stabilization of octahedrally coordinated  $\text{Cr}^{3+}$  attained in rather

refractory and close packed oxide<sup>[33]</sup>. The YAG CF was then inserted into a fused silica capillary with 76- and 320- $\mu\text{m}$  inner and outer diameters for the co-drawing process by the same LHPG system to form the double-clad structure. The 1970 °C melting temperature of the YAG is comparable to the 1600 °C soften temperature of the fused silica. The heating of the co-drawing LHPG method caused a strong interdiffusion between the YAG core and the fused-silica capillary, resulting in an inner cladding layer made of the mixtures. In particular, the DCF core diameter can be well-controlled by just altering the CO<sub>2</sub> laser power and the relative growth speed.

## 2 Tunable laser using glass-clad Ti<sup>3+</sup>:sapphire crystal fiber as the gain medium

As shown in Fig. 2, an external cavity laser configuration was employed to find out the optical characteristics of the glass-clad Ti<sup>3+</sup>:sapphire CF. The input and output ends of a 24 mm glass-clad Ti<sup>3+</sup>:sapphire CF were coated with dielectric films. At the input end, it was anti-reflection coated at 520 nm and high-reflection coated at wavelengths of 715~860 nm. At the output end, it was coated with a transmittance of greater than 99% from 715 to 860 nm. A 1 W, 520 nm Laser Diode (LD) was used as the pump light source. A 60 $\times$  aspheric lens ( $f=2.8$  mm, NA=0.65, New Focus) was used to couple the pump LD into an 18  $\mu\text{m}$  crystal fiber core, followed by a achromatic lens with  $f=7.5$  cm to collimate the light. Flat output couplers with various transmittance levels were attempted. A filter (NG610, Thorlabs) was used to remove the residual pump power. The backward lasing spectrum was measured using an optical spectrum analyzer (U4000, Ocean Optics) through a dichroic mirror (LPD01-633RS-25, Semrock) to eliminate the pump wavelength.



SCCF: single-clad crystal fiber; HWP: half-wave plate; LPF: long-wavelength-pass filter; PM: power meter; BS: beam splitter; OSA: optical spectrum analyzer

Fig. 2 External-cavity crystal fiber laser configuration

To model the optical characteristics of the glass-clad Ti<sup>3+</sup>:sapphire CF, a distributed scheme on the pump, signal, and meta-stable state population is employed as shown below.

$$\pm \frac{dP_p^\pm(z)}{dz} = -[\Gamma_p N_g(z) \sigma_a + \alpha_{pl}^p] P_p^\pm(z) \quad (1)$$

$$\pm \frac{dP_s^\pm(\lambda_i, z)}{dz} = [\Gamma_s N_2(z) \sigma_e(\lambda_i) - \alpha_{pl}^s] P_s^\pm(\lambda_i, z) + N_2(z) A_{core} S_{sp}(\lambda_i) \Delta\lambda_i \quad (2)$$

$$\frac{dN_2(z, t)}{dt} = N_0(z, t) W_{03} - N_2(z, t) \left( W_{21} + \frac{1}{\tau_f} \right) \quad (3)$$

where  $P_p^\pm(z)$ ,  $P_s^\pm(\lambda_i, z)$ ,  $N_g(z)$ , and  $N_2(z)$ , respectively denote the pump and signal powers, and electron densities of the ground state and meta-stable state.  $\lambda_i$  represents each of the signal wavelength within the gain bandwidth.  $\pm$  denotes the counter propagation directions.  $\sigma_a$ ,  $\sigma_e(\lambda_i)$ ,  $\alpha_{pl}^s$ , and  $\alpha_{pl}^p$  represent the absorption and emission cross sections, and propagation losses at signal and pump wavelengths, respectively.  $\Gamma_p$  and  $\Gamma_s$  are the confinement factors.  $A_{core}$  is the crystal core area. The spontaneous emission spectral density ( $S_{sp}$ ), the transition probability of the ground-state absorption rate ( $W_{03}$ ), and the stimulated emission rate ( $W_{21}$ ) can be expressed as follows

$$S_{sp}(\lambda_i) = \frac{4\pi n_{core}(n_{core} - n_{clad})hc^2}{\lambda^5} \sigma_e(\lambda_i) \quad (4)$$

$$W_{03}(z) = \frac{I_p \sigma_a \lambda_p}{hc} \quad (5)$$

$$W_{21}(z) = \sum \frac{I_s(\lambda_i) \sigma_e(\lambda_i) \lambda_i}{hc} \quad (6)$$

where  $n_{\text{core}}$  and  $n_{\text{clad}}$  are the refractive indices of the core and cladding, respectively.  $h$  is Planck's constant.  $\lambda$ ,  $I_p$ , and  $I_s(\lambda_i)$  represent the wavelength, pump intensity, and signal intensity. According to the lifetime measurement experiment, the average  $\tau_f$  (lifetime) was 3  $\mu\text{s}$ . The pump and signal attenuation coefficients were measured at 0.946  $\text{cm}^{-1}$ , 0.017  $\text{cm}^{-1}$ , respectively.

Fig. 3 shows the comparison between measurement and simulation at various output couplers. The fitted parameters are listed in Table 1, and will be compared with those obtained from the  $\text{Cr}^{4+}:\text{YAG}$  crystal fiber.

To further study the wavelength tuning properties, a Littrow blazed grating (10RG1800-500-1, Newport) was employed as the wavelength tuning element and the output coupler, as shown in Fig. 4. Diffraction efficiency of the grating and the angular dispersion were 88% and 13.81  $\text{nm}/^\circ$ , respectively. Output powers were measured after filtering out the residual pump power by a long-wavelength-pass filter. The tuning bandwidth was 183 nm covering 693 nm to 876 nm, as depicted in Fig. 5. Continuous smooth wavelength tuning was achieved all over the wavelength range and no discontinuity nor multiple lines were observed. The tuning range was limited by the reflectance of the CF input coating.

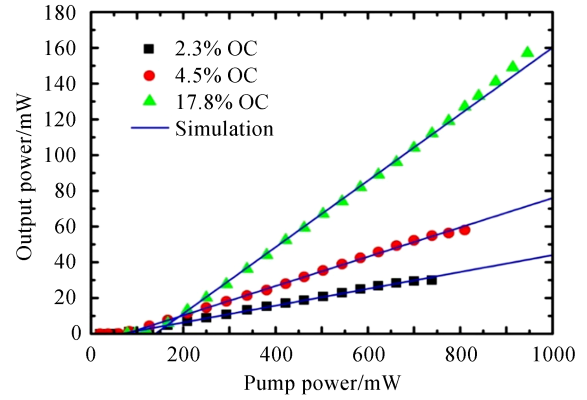
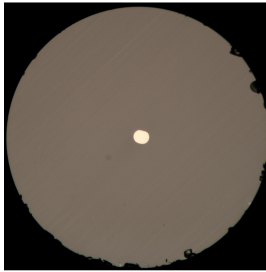
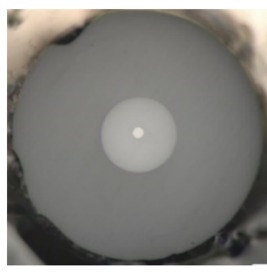


Fig. 3 Measured and simulated powers of the  $\text{Ti}^{3+}:\text{sapphire}$  SCCF lasers

**Table 1 Summary of the physical and optical properties of the glass-clad  $\text{Ti}^{3+}:\text{sapphire}$  and  $\text{Cr}^{4+}:\text{YAG}$  crystal fibers**

Parameters	Symbol	$\text{Ti}^{3+}:\text{sapphire}$	$\text{Cr}^{4+}:\text{YAG}$
Cross sectional image	—		
Core diameter	—	Short-axial: 12 $\mu\text{m}$ Long-axial: 16 $\mu\text{m}$	16 $\mu\text{m}$
Refractive index	$n$	Core: 1.77 Cladding: 1.497@446 nm	Core: 1.809 Inner-clad: 1.64 Outer-clad: 1.45@1450 nm
Active ion concentration	$N$	$1.65 \times 10^{19} \text{ cm}^{-3}$	$3.41 \times 10^{17} \text{ cm}^{-3}$
Absorption cross section	$\sigma_a$	$5.7 \times 10^{-20} \text{ cm}^2 @ 532 \text{ nm}$	$22 \times 10^{-19} \text{ cm}^2 @ 1064 \text{ nm}$
Emission cross section	$\sigma_e$	$2.4 \times 10^{-19} \text{ cm}^2 @ 790 \text{ nm}$	$2.67 \times 10^{-19} \text{ cm}^2 @ 1431 \text{ nm}$
Pump excited state absorption	$\sigma_{\text{esa}}^p$	—	$5.1 \times 10^{-19} \text{ cm}^2 @ 1064 \text{ nm}$
Signal excited state absorption	$\sigma_{\text{esa}}^e$	—	$1.28 \times 10^{-19} \text{ cm}^2 @ 1431 \text{ nm}$
Fluorescence lifetime @300 K	$\tau_f$	3.15 $\mu\text{s}$	4.2 $\mu\text{s}$
Propagation loss	$\alpha_{\text{pl}}$	0.045 dB/cm	0.027 dB/cm

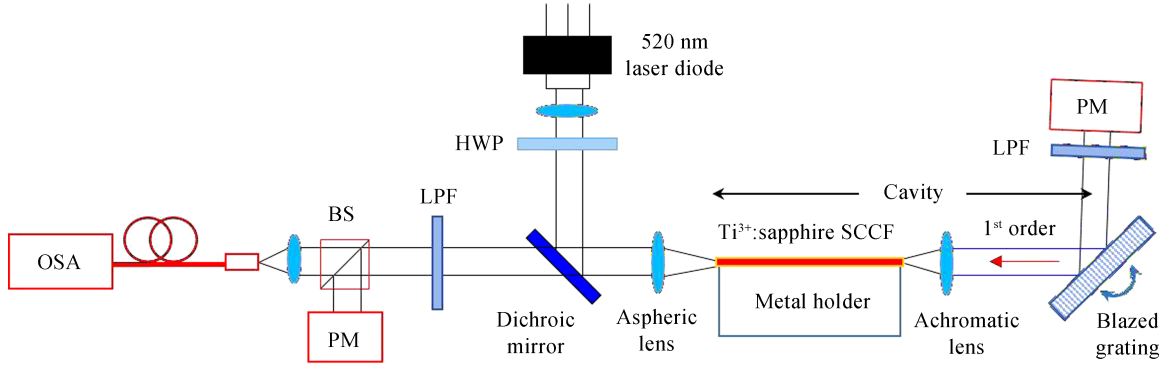


Fig. 4 Tunable  $\text{Ti}^{3+}$ :sapphire SCCF laser configuration

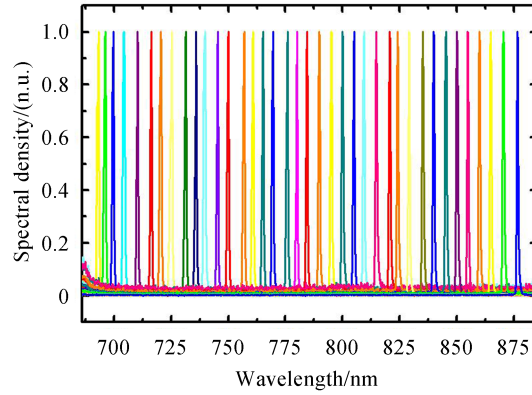


Fig. 5 Wavelength tuning spectra. Different colors represent the laser output spectra at different grating angles

To find out the tuning speed capability of the Ti:sapphire CF laser, the grating based tuning mechanism is modeled by tunable filter in a time-dependent distributed laser setting. The rotating grating is equivalent to a tunable filter with a full width at half maximum bandwidth of 2.78 nm. The governing equations of the pump and signal in Eqs. (1) and (2) are revised as Eqs. (7) and (8).

$$\pm \left[ \frac{\partial P_p^\pm(z, t)}{\partial z} \pm \frac{n}{c} \frac{\partial P_p^\pm(z, t)}{\partial t} \right] = -[\Gamma_p N_g(z, t) \sigma_a + \alpha_{pl}^p] P_p^\pm(z, t) \quad (7)$$

$$\pm \left[ \frac{\partial P_s^\pm(\lambda_i, z, t)}{\partial z} \pm \frac{n}{c} \frac{\partial P_s^\pm(\lambda_i, z, t)}{\partial t} \right] = [\Gamma_s N_2(z, t) \sigma_e(\lambda_i) - \alpha_{pl}^s] P_s^\pm(\lambda_i, z, t) + N_2(z, t) A_{core} S_{sp}(\lambda_i) \Delta\lambda_i \quad (8)$$

Depending on the rotating speed of the grating, the laser shows pulsed output with time-dependent lasing wavelength. At a pump power of 1.8 W, the simulation result with a sweep rate of 20 kHz is shown in Fig. 6.

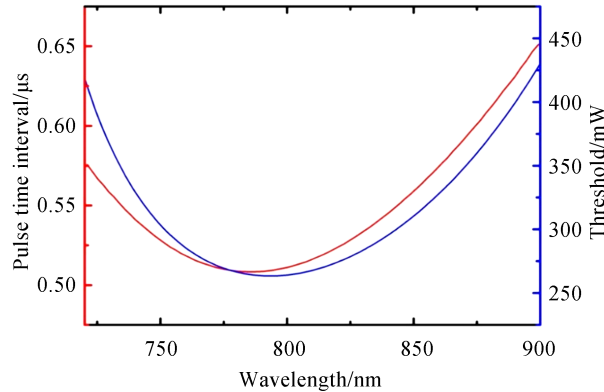


Fig. 6 Wavelength dependent threshold and pulse time interval

The typical pulse time intervals are  $0.5\sim 0.6\ \mu\text{s}$ . This represents about 2 nm spacing of the comb shaped spectra at a tuning range of 180 nm.

### 3 Tunable laser using glass-clad $\text{Cr}^{4+}$ :YAG crystal fiber as the gain medium

Compared with  $\text{Ti}^{3+}$ :sapphire CF, the  $\text{Cr}^{4+}$ :YAG CF is double-cladded.  $\text{Cr}^{4+}$ :YAG Double-Clad Crystal Fiber (DCCF) with low propagation loss ( $\sim 0.02\ \text{dB/cm}$ ) was cladded with fused silica by the sapphire-tube-assist co-drawing LHPG method<sup>[19]</sup>. At a core-diameter of 16  $\mu\text{m}$ , the stress-induced emission cross section reduction is minimized<sup>[34-35]</sup>. To develop the  $\text{Cr}^{4+}$ :YAG DCCF tunable laser, an external-cavity laser was built-up, as shown in Fig. 7. The 4.7 cm-long  $\text{Cr}^{4+}$ :YAG DCCF was pumped by a polarized 1064 nm laser diode (LD-1064-BF-600, Innolume). The DCCF was mounted on a metal holder and glued using a silver adhesive for passive heat dissipation. The input end was coated with high-reflection ( $R > 99\%$ , from 1347 to 1554 nm) dielectric thin film for broadband signal light. The signal output was collected by an aspheric lens and reflected by a planer output coupler ( $T = 4.4\%$ ). The laser output power was measured at both sides of the cavity.

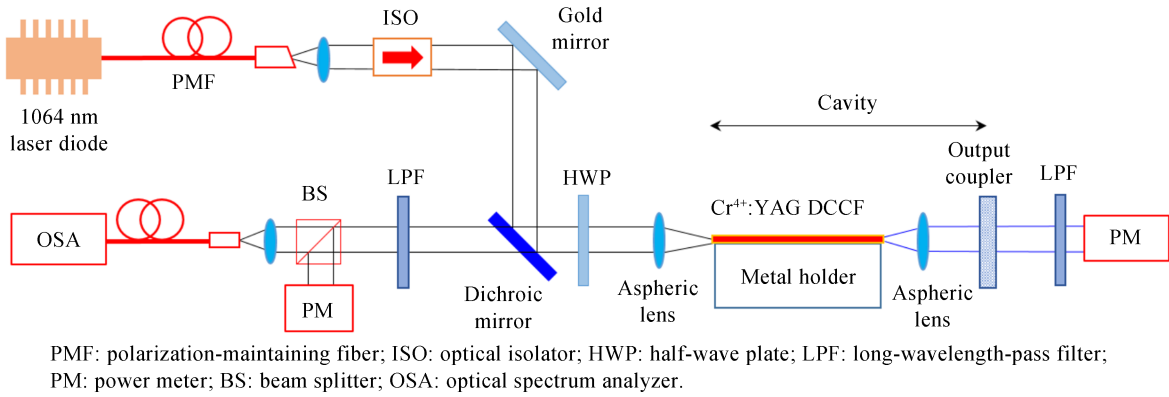


Fig. 7 Schematic of the external-cavity  $\text{Cr}^{4+}$ :YAG DCCF laser system

Fig.8 shows the measured laser output power. The threshold pump power is only 51 mW. The slope

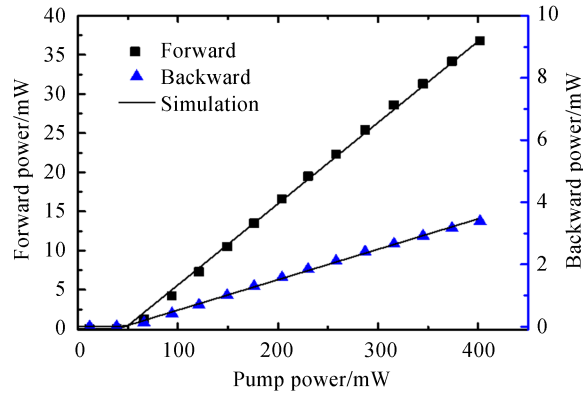


Fig. 8 Measured and simulated powers of the  $\text{Cr}^{4+}$ :YAG DCCF laser

efficiencies are 10.7% and 1.0% from the forward and backward ends, respectively. To model the laser, Eqs. (1) and (2) need to be modified with the addition of  $\text{Cr}^{4+}$ :YAG's Excited State Absorption (ESA). The distributed simulation model is described in Section 2 with the addition of the ESA terms in Eqs. (9) and (10). The experimental result agrees well with the simulation.

$$\pm \frac{dP_p^\pm(z)}{dz} = -[\Gamma_p(N_g(z)\sigma_a + N_2(z)\sigma_{esa}^p) + \alpha_{pl}^p]P_p^\pm(z) \quad (9)$$

$$\pm \frac{dP_s^\pm(\lambda_i, z)}{dz} = [\Gamma_s N_2(z) [\sigma_e(\lambda_i) - \sigma_{esa}^s(\lambda_i)] - \alpha_{pl}^s]P_s^\pm(\lambda_i, z) + N_2(z) A_{core} S_{sp}(\lambda_i) \Delta\lambda_i \quad (10)$$

where  $\sigma_{\text{esa}}^p$  and  $\sigma_{\text{esa}}^s$  are the pump and signal ESA cross sections, respectively.

Table 1 summarizes the simulation parameters of the  $\text{Ti}^{3+}$ :sapphire SCCF and  $\text{Cr}^{4+}$ :YAG DCCF lasers. Though the  $\text{Cr}^{4+}$  concentration ( $3.41 \times 10^{17} \text{ cm}^{-3}$ ) is about 2 orders of magnitude less than that of the  $\text{Ti}^{3+}$ , the  $\text{Cr}^{4+}$ 's high absorption cross section avoids the need for a long  $\text{Cr}^{4+}$ :YAG DCCF. The high pump and signal ESAs do not significantly affect the  $\text{Cr}^{4+}$ :YAG DCCF laser efficiency; however, it does limit the tuning bandwidth of  $\text{Cr}^{4+}$ :YAG laser, and it will be discussed below.

The setup of the  $\text{Cr}^{4+}$ :YAG crystal fiber tunable laser is shown in Fig. 9. A reflective holographic Littrow-configured grating (53004BK02-246H, Richardson Grating) operated at the 1<sup>st</sup>-order diffraction was used as the tuning element and output coupler. The grating with a pitch density of 1 050 pairs/mm has high diffraction efficiency ( $\sim 97\%$ ) in 1.3 to 1.6  $\mu\text{m}$ .

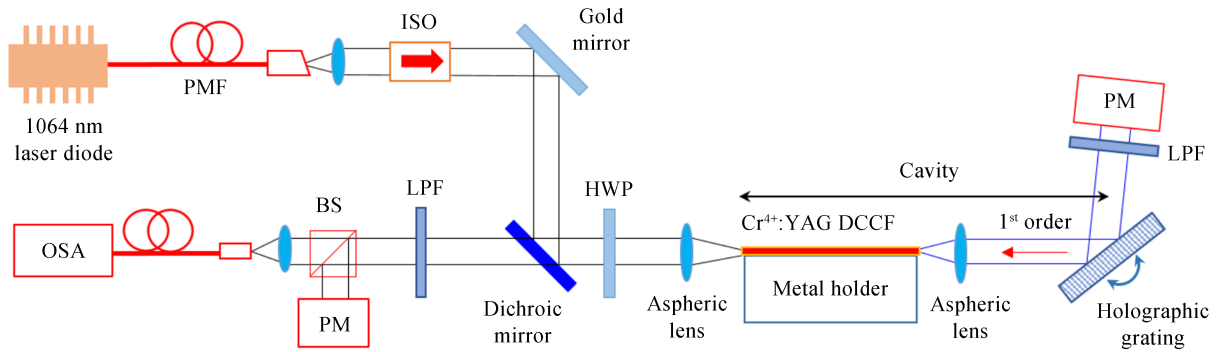


Fig. 9 Schematic of the  $\text{Cr}^{4+}$ :YAG DCCF based tunable laser

Fig. 10 shows the output characteristics of the  $\text{Cr}^{4+}$ :YAG DCCF tunable laser. The threshold was less than 100 mW, which was more than one order lower than non-CF based  $\text{Cr}^{4+}$ :YAG lasers in literature. The linewidth was 0.029 nm. The spectrum of the individual wavelength shown in Fig. 11 was recorded by the optical spectrum analyzer every few nanometers. In Fig. 11, the tuning range was 170 nm, from 1 353 to 1 523 nm. In all tuning range, the side-mode suppression ratio was more than 45 dB. It should be noted that the  $\text{Cr}^{4+}$ :YAG DCCF tunable laser exhibited narrow linewidth and low amplified spontaneous emission noise compared to the Bismuth-doped fiber tunable laser operated in similar wavelength range<sup>[36]</sup>.

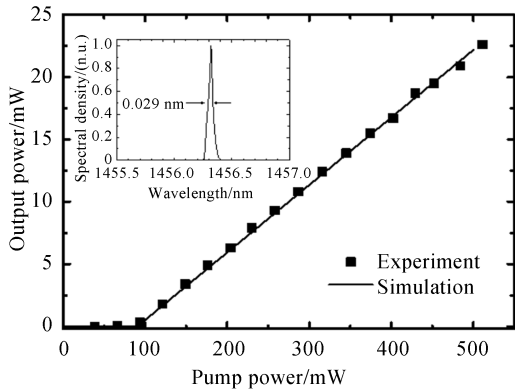


Fig. 10 The laser performance at 1 456 nm. The inset shows the linewidth of 0.029 nm

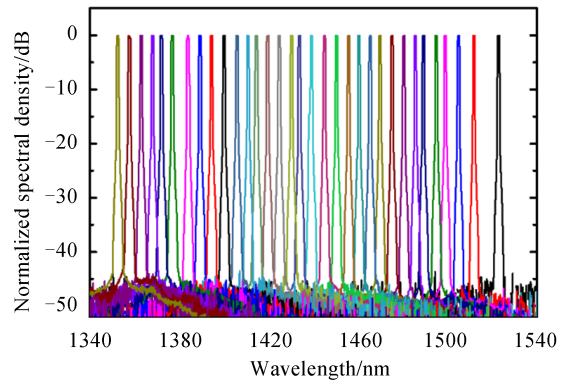


Fig. 11 Wavelength tuning spectra. Different colors represent the laser output spectra at different grating angles

The tuning ranges at different pump powers were measured as shown in Fig. 12. The maximum tuning range of 170 nm (1 353 to 1 523 nm) was occurred at 232 mW pumping power. Then, the tuning range decreased to 150 nm and became stable at 150 nm when increasing the pump power. It was due to the signal ESA at longer wavelength with high intensity in the  $\text{Cr}^{4+}$ :YAG DCCF. To reveal the limitation, the gain of the  $\text{Cr}^{4+}$ :YAG DCCF is numerically simulated. The tuning range becomes larger with the increasing gain. After 300 mW pump power, the tuning range became stable and the gain gradually saturated. The ESA limitation



near the long-wavelength end could be mitigated by longer DCCF or higher concentration.

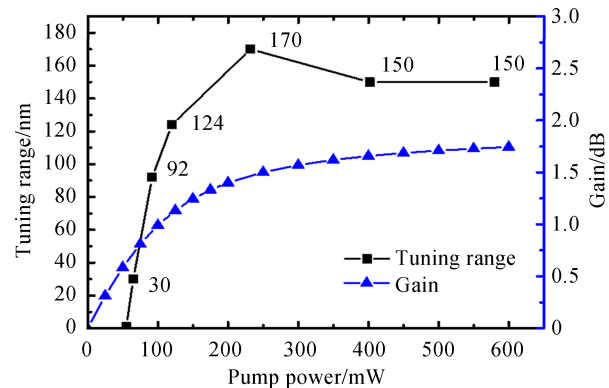


Fig. 12 The relationship between the tuning range and the gain of the  $\text{Cr}^{4+}$ :YAG DCCF

## 4 Conclusion

Forth years had been past since the first active CF was grown. Due to the superior optical, mechanical, and thermal properties, CF based light sources have shown advantages in areas where high power and high brightness are needed. It is advantageous to draw transition-metal-ions doped crystals into fiber so that the heat dissipation, pump/signal interaction can be improved for efficient laser operation. Both  $\text{Ti}^{3+}$ :sapphire SCCF and  $\text{Cr}^{4+}$ :YAG DCCF have shown tuning range of greater than 170 nm at relatively low pump powers. Though the gains of transition-metal-ions doped solid-state laser crystals are in general much less than the semiconductor lasers, fast wavelength sweep is still quite feasible at tens of kHz speed for various applications.

For future ultra-broadband fiber communication system, a broadly tunable laser is essential to offer wavelength-on-demand, dynamic wavelength ports, and simplified inventory managements. In the emerging biomedical imaging field, optical coherence tomography has now become a standard of care impacting the treatment of millions of people every year. Due to the breakthroughs in broadband light sources for reaching the deep and/or interior tissues and organs, cellular-resolution optical coherence tomography could enable optical virtual biopsy in future.

At present, it is challenging to develop a single-mode glass-clad CF mainly due to the large indices of refraction of YAG and sapphire crystals. Using solution based dip coating techniques on CF, followed by high temperature sintering process, could be a viable way to fabricate a fully crystalline clad for single-mode transmission. Such a fully crystalline core and clad fiber could also escalate the optical damage thresholds of the silica fiber based lasers, and could further enable novel applications.

## References

- [1] KAO K C, HOCKHAM G A. Dielectric-fibre surface waveguides for optical frequencies[J]. *Proceedings of the Institution of Electrical Engineers*, 1966, **113**(7): 1151-1158.
- [2] MEARS R J, REEKIE L, JAUNCEY I M, *et al.* Low-noise erbium-doped fibre amplifier operating at 1.54  $\mu\text{m}$  [J]. *Electronics Letters*, 1987, **23**(19): 1026-1028.
- [3] HUANG D, SWANSON E A, LIN C P, *et al.* Optical coherence tomography[J]. *Science*, 1991, **254**(5035): 1178-1181.
- [4] DREXLER W, MORGNER U, KRTNER F X, *et al.* In vivo ultrahigh-resolution optical coherence tomography [J]. *Optics Letters*, 1999, **24**(17): 1221-1223.
- [5] MCCUMBER D E. Theory of phonon terminated optical masers[J]. *Physical Review*, 1964, **134**(2A): A299-A306.
- [6] WU C J. Room-temperature broadly tunable laser crystals[J]. *Journal of Synthetic Crystals*, 1993, **22**(4): 384-390.
- [7] SIEGMAN A E. Lasers[M]. California: University Science Books Sausalito, 1986.
- [8] ANDERSON A A, EASON R W, HICKEY L M B, *et al.* Ti:sapphire planar waveguide laser grown by pulsed laser deposition[J]. *Optics Letters*, 1997, **22**(20): 1556-1558.
- [9] BURRUS C A, STONE J. Single-crystal fiber optical devices: A Nd:YAG fiber laser[J]. *Applied Physics Letters*, 1975, **26**(6): 318-320.
- [10] BURRUS C A, STONE J, DENTAI A G. Room-temperature 1.3  $\mu\text{m}$  CW operation of a glass-clad Nd:YAG single-

- crystal fiber laser end pumped with a single LED[J]. *Electronics Letters*, 1976, **12**(22): 600-602.
- [11] FEJER M M, NIGHTINGALE J L, MAGEL G A, *et al.* Laser-heated miniature pedestal growth apparatus for single-crystal optical fibers[J]. *Review of Scientific Instruments*, 1984, **55**(11): 1791-1796.
- [12] FEIGELSON R S. Pulling optical fibers[J]. *Journal of Crystal Growth*, 1986, **79**(1-3): 669-680.
- [13] HUO Y, LI G, DUAN Y, *et al.* Crystal optical fiber laser with linearly polarized output[C]. CLEO, 1991:CThL4.
- [14] DUAN Y, HUO Y, HUANG Z, *et al.* Laser-diode-pumped Nd:YAP single crystal fiber laser[J]. *Chinese Optics Letters*, 1991, **8**(12): 622-624.
- [15] HUANG S L. Crystalline fibers for fiber lasers and amplifiers[M]. In: G. D. Peng (eds) Handbook of Optical Fibers, Singapore: Springer, 2019.
- [16] LO C Y, HUANG K Y, CHEN J C, *et al.* Glass-clad Cr<sup>4+</sup>:YAG crystal fiber for the generation of superwideband amplified spontaneous emission[J]. *Optics Letters*, 2004, **29**(5): 439-441.
- [17] HUANG Y C, LU Y K, CHEN J C, *et al.* Broadband emission from Cr-doped fibers fabricated by drawing tower[J]. *Optics Express*, 2006, **14**(19): 8492-8497.
- [18] CHEN J C, LIN Y S, TSAI C N, *et al.* 400-nm-bandwidth emission from a Cr-doped glass fiber[J]. *IEEE Photonics Technology Letters*, 2007, **19**(8): 595-597.
- [19] HUANG K Y, HSU K Y, JHENG D Y, *et al.* Low-loss propagation in Cr<sup>4+</sup>:YAG double-clad crystal fiber fabricated by sapphire tube assisted CDLHPG technique[J]. *Optics Express*, 2008, **16**(16): 12264-12271.
- [20] WANG S C, YANG T I, JHENG D Y, *et al.* Broadband and high-brightness light source: Glass-clad Ti:sapphire crystal fiber[J]. *Optics Letters*, 2015, **40**(23): 5594-5597.
- [21] MOULTON P. Ti-doped sapphire: tunable solid-state laser[J]. *Optics News*, 1982, **8**(6): 9.
- [22] IZAWA T, MATSUI S, MAEDA M, *et al.* Broad-band tunable, compact, low-threshold, Ti:sapphire laser using a single set of extremely broad-band optics[C]. CLEO, 1996: CtuL27.
- [23] GRIVAS C, CORBARI C, BRAMBILLA G, *et al.* Tunable, continuous-wave Ti:sapphire channel waveguide lasers written by femtosecond and picosecond laser pulses[J]. *Optics Letters*, 2012, **37**(22): 4630-4632.
- [24] ANGERT N B, BORODIN N I, GARMASH V M, *et al.* Lasing due to impurity color centers in yttrium aluminum garnet crystals at wavelengths in the range 1.35-1.45  $\mu\text{m}$ [J]. *Soviet Journal of Quantum Electronics*, 1988, **18**(1): 73-74.
- [25] EILERS H, DENNIS W M, YEN W M, *et al.* Performance of a Cr:YAG laser[J]. *IEEE Journal of Quantum Electronics*, 1993, **29**(9): 2508-2512.
- [26] SOROKINA I T, NAUMOV S, SOROKIN E, *et al.* Directly diode-pumped tunable continuous-wave room-temperature Cr<sup>4+</sup>:YAG laser[J]. *Optics Letters*, 1999, **24**(22): 1578-1580.
- [27] SENNAROGLU A. Broadly tunable Cr<sup>4+</sup>-doped solid-state lasers in the near infrared and visible [J]. *Progress in Quantum Electronics*, 2002, **26**(6): 287-352.
- [28] ISHIBASHI S, NAGANUMA K. Cr<sup>4+</sup>:YAG single-crystal fiber laser widely tunable using birefringent filter[C]. CLEO, 2012: JW2A.
- [29] JHENG D Y, HSU K Y, LIANG Y C, *et al.* Broadly tunable and low-threshold Cr<sup>4+</sup>:YAG crystal fiber laser[J]. *IEEE Journal of Selected Topics in Quantum Electronics*, 2015, **21**(1): 0900608.
- [30] YANG T T, YANG T I, SOUNDARARAJAN R, *et al.* Widely tunable, 25-mW power, Ti:sapphire crystal-fiber laser [J]. *IEEE Photonics Technology Letters*, 2019, **31**(24): 1921-1924.
- [31] LAI C C, KE C P, LIU S K, *et al.* Intracavity and resonant Raman crystal fiber laser[J]. *Applied Physics Letters*, 2012, **100**: 261101.
- [32] CHEN P Y, CHANG C L, HUANG K Y, *et al.* Experiment and simulation on interface shapes of an yttrium aluminium garnet miniature molten zone formed using the laser-heated pedestal growth method for single-crystal fibers[J]. *Journal of Applied Crystallography*, 2009, **42**(4): 553-563.
- [33] JI J Y, SHEN P, CHEN J C, *et al.* On the deposition of Cr<sub>3</sub>- $\delta$ O<sub>4</sub> spinel particles upon laser heated pedestal growth of Cr:YAG fiber[J]. *Journal of Crystal Growth*, 2005, **282**: 343-352.
- [34] LAI C C, KE C P, LIU S K, *et al.* Efficient and low-threshold Cr<sup>4+</sup>:YAG double-clad crystal fiber laser[J]. *Optics Letters*, 2011, **36**(6): 784-786.
- [35] LAI C C, YE H P, WANG S C, *et al.* Strain-dependent fluorescence spectroscopy of nanocrystals and nanoclusters in Cr:YAG crystalline-core fibers and its impact on lasing behavior[J]. *Journal of Physical Chemistry C*, 2012, **116**(49): 26052-26059.
- [36] PARAMONOV V M, BELOVOLOV M I, KHOPIN V F, *et al.* Bismuth-doped fibre laser continuously tunable within the range from 1.36 to 1.51  $\mu\text{m}$ [J]. *Quantum Electronics*, 2016, **46**(12): 1068-1070.